SU(4) Symmetry in Twisted Bilayer Graphene: An Itinerant Perspective

Dmitry V. Chichinadze,[1] Laura Classen,[2] Yuxuan Wang,[3] and Andrey V. Chubukov[1]
[1]School of Physics and Astronomy, University of Minnesota, Minneapolis, Minnesota 55455, USA
[2]Condensed Matter Physics and Materials Science Division, Brookhaven National Laboratory, Upton, New York 11973, USA
[3]Department of Physics, University of Florida, Gainesville, Florida 32601, USA

(Received 11 August 2021; accepted 10 May 2022; published 3 June 2022)

We study symmetry-broken phases in twisted bilayer graphene at small filling above charge neutrality and at van Hove filling. We argue that the Landau functionals for the particle-hole order parameters at these fillings both have an approximate SU(4) symmetry, but differ in the sign of quartic terms. We determine the order parameter manifold of the ground state and analyze its excitations. For small fillings, we find a strong first-order transition to an $\mathrm{SU}(3) \otimes \mathrm{U}(1)$ manifold of orders that break spin-valley symmetry and induce a 3-1 splitting of fermionic excitations. For van Hove filling, we find a weak first-order transition to an $\mathrm{SU}(2) \otimes \mathrm{SU}(2) \otimes \mathrm{U}(1)$ manifold of orders that preserves the twofold band degeneracy. We discuss the effect of particle-hole orders on superconductivity and compare with strong-coupling approaches.

DOI: 10.1103/PhysRevLett.128.227601

Introduction.—Twisted bilayer graphene (TBG) is a correlated electron system near a particular "magic" twist angle between the layers $\theta \sim 1°$, where the (quasi)periodic moire pattern with length scale of order 14 nm yields nearly flat bands separated from the rest of the energy spectrum by a gap of about 40 meV [1,2]. This system has attracted enormous interest in the last few years because it displays superconductivity [3–8] and correlated insulating phases [1,6,9–17] near integer filling factors $|n| = 1, 2, 3$.

A popular theoretical approach to TBG is to treat it as a system in which Coulomb interaction well exceeds the kinetic energy (see, e.g., [18–25] and references therein). Within this approach, the ground states at $|n| = 1, 2, 3$ are correlated insulators with distinct broken symmetries and band topology, the fermionic spectra consist of energy levels [21] or narrow bands, induced by the interaction [24].

In this Letter, we use as the point of departure, the experimental observations [1,3–5,8,12,13,15–17,26–31] that in between integer fillings TBG displays metallic behavior and study instabilities in a particle-hole channel near an integer n. We show that the corresponding order splits and reconstructs the bands and may eventually drive the system into an insulating phase with narrow subbands. The rationale for our approach comes from STM data [12,13,16,26], which show that the density of states is nonzero everywhere in the flat region and displays van Hove (vH) singularities, expected in the band spectrum for itinerant fermions, and from transport data, which show that the conductivity displays metallic behavior away from integer fillings [1,3–5,8,15,17,27].

Our key results are an emergent SU(4) symmetry of itinerant fermions, which has also been argued to exist in strong-coupling approaches, and the identification of the manifold of degenerate ordered states, resulting from breaking of SU(4). We argue that the manifold is different near different n. This gives rise to different degeneracies of reconstructed fermionic levels. We model the behavior near two exemplary n by introducing patch models for typical Fermi surface geometries: pockets around the K, K' points at small filling, and vH points at intermediate filling. We emphasize that these features are insensitive to the details of the band structure. We will also analyze which orders are detrimental to superconductivity and which are not. We do not address topological properties, as the patch approximation excludes Dirac points. We conjecture that the same orders that we find based on symmetry and universal properties of the dispersion, can be extended beyond the patch approximation and give rise to proper topological behavior.

Model.—The narrow spectrum of TBG contains four bands (two with positive and two with negative energy, counted from charge neutrality), each is spin degenerate. We use the band dispersion, obtained in numerical simulations on TBG [32–34], and the Kang-Vafek model [18,35] for four-fermion interactions, which includes density-density interactions and additional exchangelike interactions within a hexagon in the moire lattice. For definiteness, we consider electron doping and focus on the two bands with positive energy. The bands are specified by the original valley index and are nondegenerate for a generic momentum. We analyze two cases: (i) vH filling, when the chemical potential passes through three vH points per valley and the density of states diverges logarithmically, or even more strongly for specific band parameters [36] [the six-patch model, Fig. 1(a)] and (ii) smaller filling, when the Fermi surface is sizable, but still consists of pockets, centered at Dirac points K and K', [the two-patch model, Fig. 1(b)]. We apply the six-patch model to $n \approx 2$,

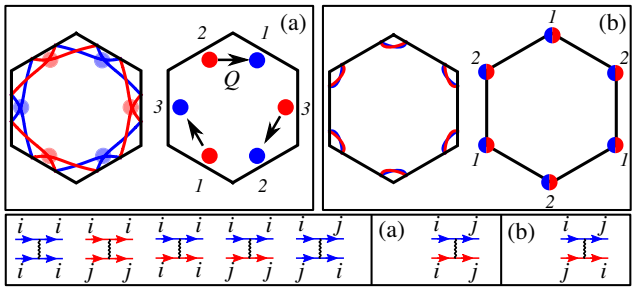

FIG. 1. Patch models and relevant interactions. Red and blue are fermions from the two valleys. (a) Six-patch model at vH filling ($i, j = 1$–3 label patches). (b) Two-patch model. Lower panel: four-fermion interactions. On the right are interactions, common to both models. Equal interactions are shown once. On the left are interactions, specific to six-patch (a) and two-patch model (b).

which experimentally is close to vH filling, and the two-patch model to fillings around $n = 1$. In each case we identify the set of leading particle-hole instabilities and obtain the reconstructed fermionic spectrum.

SU(4) symmetry for itinerant fermions.—A generic particle-hole order parameter $\Phi_{ij}(\mathbf{k}, \mathbf{Q})$, made out of two fermions, is specified by fermionic momenta $\mathbf{k}$ and $\mathbf{k} + \mathbf{Q}$ and two Pauli matrices: σ_i acting in spin space, and τ_i acting in "isospin" valley space ($i, j = 0, 1, 2, 3$, where σ_0 and τ_0 are identity matrices). The effective Hamiltonian for the coupling between $\Phi_{ij}(\mathbf{k}, \mathbf{Q})$ and fermions can be cast into a 4×4 matrix form

$$\mathcal{H}_\Phi = \sum_{i,j,\mathbf{Q},\mathbf{k}} \Phi_{ij}(\mathbf{k}, \mathbf{Q}) c^\dagger_{\mathbf{k}} \sigma_i \otimes \tau_j c_{\mathbf{k}+\mathbf{Q}}, \tag{1}$$

where $c^\dagger$, c are creation and annihilation operators of fermions. The term with $\mathbf{Q} = 0$ and $\sigma_0 \otimes \tau_0$ can be discarded as it just renormalizes the chemical potential. For a given filling, order parameters with certain $\mathbf{Q}$'s are most likely to develop. These are, besides $\mathbf{Q} = 0$, the various $\mathbf{Q}$'s connecting different vH points for the six-patch model, and $\mathbf{Q} = \mathbf{K} - \mathbf{K}'$ for the two-patch model. The $\mathbf{k}$ dependence can be classified by irreducible representations of the lattice point group, which are often associated with, e.g., s- or d-wave symmetry. In the six-patch model, the total number of components of $\Phi_{ij}(\mathbf{k}, \mathbf{Q})$ is 143 (23 for $Q = 0$ and 120 for finite Q). In the two-patch model, there are 31 fermionic bilinears with $Q = 0$ and 32 with $Q = \mathbf{K} - \mathbf{K}'$. Each order parameter gets renormalized by the interaction as $\Phi_{ij}(\mathbf{k}, \mathbf{Q}) = \Phi^{(0)}_{ij}(\mathbf{k}, \mathbf{Q})/[1 - \lambda_{ij}(\mathbf{k}, \mathbf{Q})]$, where the dimensionless λ_{ij} depends on the coupling and (temperature-dependent) susceptibility for the ordering channel. It depends on the model, which coupling(s) induce the leading instability upon lowering the temperature at $\lambda_{i,j} \to 1$.

In the six-patch model the two largest couplings correspond [30] to a seven-component intravalley spin and charge order ($Q = 0$, s-wave symmetry, $i = 0, \ldots, 3$, $j = 0, 3$ with $i = j = 0$ excluded) and an eight-component intervalley spin- and charge-density-wave order ($Q \neq 0$ connects neighboring vH points, s-wave symmetry, $i = 0, \ldots, 3$, $j = 1, 2$). The two couplings are not identical, but are numerically very close for an arbitrary ratio of the density-density and the TBG-specific exchange components of the interaction. Neglecting the difference, we end up with the model of 15 order parameters specified by 15 4×4 matrices $\sigma_i \otimes \tau_j$. These 15 matrices can be viewed as orthonormal generators of an SU(4) group, and 15 corresponding order parameters form the adjoint representation of SU(4). The free energy at the quadratic level is the sum of the squares of these 15 order parameters [37]. We emphasize that SU(4) is an emergent symmetry of the order parameter manifold, and the full low-energy itinerant model is not SU(4) symmetric. We verified [38] that the same approximate SU(4) symmetry, appears in the model with 12 vH points, which may be relevant to $n = -2$.

A similar situation holds for the two-patch model near $n = 1$. Here we find [38] that 15 $Q = 0$ order parameters, symmetric between patches at K and K', have the largest and identical couplings. Neglecting other bilinears, we again obtain an effective model, described by 15 orthonormal generators of SU(4), with 15 order parameters forming the adjoint representation. In both models, the order parameters can be relabeled as one scalar field $\phi = \Phi_{0,3}$, two vector fields $\boldsymbol{S}_+ = \Phi_{i,0}$ and $\boldsymbol{S}_- = \Phi_{i,3}$, two intervalley scalar fields $\phi_{A,B} = \Phi_{0,j}$, and two intervalley vector fields $\boldsymbol{S_A}$, $\boldsymbol{S_B} = \Phi_{i,j}$ ($i = 1, \ldots, 3$, $j = 1, 2$).

SU(4) Landau functional.—To derive the Landau functional, we depart from the model of interacting fermions with dispersion appropriate for vH and smaller filling. We introduce 15 order parameters in each case, use a Hubbard-Stratonovich transformation to integrate out fermions, and expand the free energy in powers of the order parameters, with coefficients evaluated using propagators of patch fermions [38]

$$F = \frac{\alpha}{4}\mathrm{Tr}(\Phi^2) + \frac{3\gamma}{\sqrt{2}}\mathrm{Tr}(\Phi^3) + \frac{\beta}{4}\mathrm{Tr}(\Phi^4) + \mathcal{O}(\Phi^6), \tag{2}$$

where $\Phi \equiv \sum_{\{i,j\}} \Phi_{ij} \sigma_i \otimes \tau_j$, and prefactors α, β, and γ are different for the two- and six-patch model [40]. One can verify that F remains invariant under $\Phi \to \Phi' = U\Phi U^\dagger$ for $U \in \mathrm{SU}(4)$. Explicitly, the quadratic term has the form $F^{(2)} = \alpha R^2$, where $R^2 = \phi^2 + \phi_A^2 + \phi_B^2 + \boldsymbol{S}_+^2 + \boldsymbol{S}_-^2 + \boldsymbol{S}_A^2 + \boldsymbol{S}_B^2$. The prefactor α is expressed via the interaction and fermionic polarization, and becomes negative below some T_{ph}. The cubic term is allowed by symmetry and has the form

$$F^{(3)} = 6\sqrt{2}\gamma[\boldsymbol{S}_+ \cdot (\phi_A \boldsymbol{S}_A + \phi_B \boldsymbol{S}_B) + \phi \boldsymbol{S}_+ \cdot \boldsymbol{S}_- + \boldsymbol{S}_- \cdot \boldsymbol{S}_B \times \boldsymbol{S}_A],$$

where $\gamma = -\int G^3$, and G is a fermion propagator. One can easily verify that $\gamma = (-1/2)d^2n/d\mu^2$, where n is electronic density per spin. The presence of $F^{(3)}$ implies that the transition is first order. However, it is a weak first-order transition because γ vanishes if we expand the dispersion to the lowest order around patch points, and we expect it to be small if we go beyond the patch model and include higher-order terms. The key physics then comes from the quartic term, which is $F^{(4)} = \beta(R^4 + 4C)$, where

$$\begin{aligned} C = {} & (\boldsymbol{S}_+ \cdot \boldsymbol{S}_-)^2 + (\boldsymbol{S}_B \times \boldsymbol{S}_A + \phi \boldsymbol{S}_+)^2 + (\boldsymbol{S}_A \times \boldsymbol{S}_- + \phi_B \boldsymbol{S}_+)^2 \\ & + (\boldsymbol{S}_- \times \boldsymbol{S}_B + \phi_A \boldsymbol{S}_+)^2 + (\boldsymbol{S}_A \cdot \boldsymbol{S}_+)^2 \\ & + (\boldsymbol{S}_B \cdot \boldsymbol{S}_+)^2 + (\boldsymbol{S}_A \phi_A + \boldsymbol{S}_B \phi_B + \boldsymbol{S}_- \phi)^2. \end{aligned} \tag{3}$$

The crucial difference between the two- and six-patch models is the sign of $\beta(T)$. At vH filling (six-patch model) $\beta(T)$ is positive and diverges as $1/T^2$ at $T \to 0$. At smaller filling (two-patch model), we find $\beta(T) < 0$ at relevant T, see Figs. 5 and 7 in [38]. The difference in the sign of β has a strong impact on the type of the ordering transition and the order parameter manifold.

vH filling ($\beta > 0$).—In $F^{(4)} = \beta R^4 + 4\beta C$, the term C contains the sum of full squares. For positive β, the Landau functional is then minimal if $C = 0$, i.e., when the order parameters satisfy

$$\begin{aligned} (\boldsymbol{S}_+ \cdot \boldsymbol{S}_-) &= (\boldsymbol{S}_A \cdot \boldsymbol{S}_+) = (\boldsymbol{S}_B \cdot \boldsymbol{S}_+) \\ &= (\boldsymbol{S}_A \phi_A + \boldsymbol{S}_B \phi_B + \boldsymbol{S}_- \phi) = 0, \\ (\boldsymbol{S}_B \times \boldsymbol{S}_A + \phi \boldsymbol{S}_+) &= (\boldsymbol{S}_A \times \boldsymbol{S}_- + \phi_B \boldsymbol{S}_+) \\ &= (\boldsymbol{S}_- \times \boldsymbol{S}_B + \phi_A \boldsymbol{S}_+) = 0. \end{aligned} \tag{4}$$

For any configuration that satisfies (4), $F = \alpha R^2 + \beta R^4$, and minimizing at $T < T_{ph}$, we obtain the nonzero value of the total $R^2 = |\alpha|/(2\beta)$. The transition is second order without $F^{(3)}$ and weakly first order if the prefactor γ in $F^{(3)}$ is small but finite. We give a general parameterization for the configurations at the minimum in [38]. Specific examples are, e.g., configurations with only intravalley components ϕ and $\boldsymbol{S}_\pm$ or only intervalley components $\phi_{A,B}$ and $\boldsymbol{S}_{A,B}$. For intravalley order, there are two solutions: (i) $\phi \neq 0$, $\boldsymbol{S}_\pm = 0$ and (ii) $\phi = 0$, $\boldsymbol{S}_+ \cdot \boldsymbol{S}_- = 0$ with fixed $\boldsymbol{S}_+^2 + \boldsymbol{S}_-^2 = |\alpha|/2\beta$. The first describes s^{+-} valley order (splitting of chemical potentials for the two valleys), the second describes magnetic order with equal magnitudes of $\boldsymbol{S}_{1,2} = (\boldsymbol{S}_+ \pm \boldsymbol{S}_-)/\sqrt{2}$ in the two valleys, $\boldsymbol{S}_1^2 = \boldsymbol{S}_2^2 = |a|/4\beta$, and arbitrary angle between $\boldsymbol{S}_1$ and $\boldsymbol{S}_2$. The two limiting cases are ferromagnetic and antiferromagnetic alignments

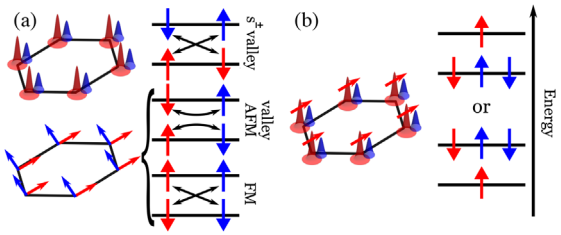

FIG. 2. A sketch of intravalley orders near $n = 2$ (a) and $n = 1$ (b). Left columns of panels (a) and (b) sketch electronic orders on the moire superlattice cell (depicted by black hexagon). Two valleys are labeled by colors (red and blue). Arrows indicate spin order for two valleys, and peaks indicate the electron density. Note that for $n = 1$, spin order develops only in one valley and is accompanied by s^{+-} density valley order. Right columns of panels (a) and (b) show possible structures of energy levels for the ordered states. Double-headed arrows indicate time-reversal-partner states. For $n = 1$, cubic terms select between the two choices (see text).

[41]. Configurations with only intervalley components describe density waves and loop currents [30]. For a generic order parameter that satisfies $F^{(4)} = \beta R^4$, nine variables remain undetermined by Eq. (4). Because the total R^2 is fixed, there are eight Goldstone modes. This can be also seen by noticing that the SU(4) symmetry is broken down to SU(2) ⊗ SU(2) ⊗ U(1). The broken symmetry is described by the coset SU(4)/[SU(2) ⊗ SU(2) ⊗ U(1)] with $15 - 6 - 1 = 8$ generators, which are the eight Goldstone modes [38].

Smaller filling ($\beta < 0$).—For negative β, the order parameter manifold is different as now one has to find configurations that *maximize* C in (3). To get a first insight, consider a configuration with only intravalley orders ϕ and $\boldsymbol{S}_\pm$. A straightforward analysis shows that in this case $F^{(4)} = -\frac{7}{3}|\beta|R^4 + |\beta|\tilde{C}$, where

$$\tilde{C} = (\boldsymbol{S}_+^2 - \boldsymbol{S}_-^2)^2 + \frac{1}{3}(2\phi^2 - \boldsymbol{S}_+^2 - \boldsymbol{S}_-^2)^2 + 4[\boldsymbol{S}_+ \times \boldsymbol{S}_-]^2. \tag{5}$$

The minimum of $F^{(4)}$ is reached when $\tilde{C} = 0$, which holds when density and spin valley orders are both nonzero: $\phi^2 = \boldsymbol{S}_+^2 = \boldsymbol{S}_-^2$ and $\boldsymbol{S}_+ = \pm \boldsymbol{S}_-$. The last condition implies that the spin order now develops only in one valley, along with s^{+-} valley order, see Fig. 2. The transition is strongly first order, and to get the equilibrium value of R^2 one needs to include sixth-order terms in Φ.

We extended this analysis to the full set of 15 order parameters by expanding around one of these states with $\phi = S_+^z = S_-^z$ to second order in $\phi_{A,B}$ and $\boldsymbol{S}_A, \boldsymbol{S}_B$. We found after long algebra that (i) the minimum of $F^{(4)}$ is still at $-(7/3)|\beta|R^4$, and (ii) the order parameter manifold at the minimum is parameterized in terms of Hopf coordinates and variables ε and r as

$$\boldsymbol{S}_+ = r\left(0,0,1-\frac{\varepsilon^2}{2}\sin^2\theta\right)$$

$$\boldsymbol{S}_A = r\varepsilon(\sin\theta\cos\psi_1, \sin\theta\sin\psi_1, \cos\theta\cos\psi_2);$$

$$\boldsymbol{S}_B = r\varepsilon(\sin\theta\sin\psi_1, -\sin\theta\cos\psi_1, -\cos\theta\sin\psi_2);$$

$$\phi = r\left(1-\frac{\varepsilon^2}{2}\right); \quad \phi_A = r\varepsilon\cos\theta\cos\psi_2;$$

$$\phi_B = -r\varepsilon\cos\theta\sin\psi_2;$$

$$\boldsymbol{S}_- = r\left(-\frac{\varepsilon^2}{2}\sin 2\theta\cos\psi_+, -\frac{\varepsilon^2}{2}\sin 2\theta\sin\psi_+, 1-\frac{\varepsilon^2}{2}\cos^2\theta\right),$$

where $\psi_+ = \psi_1 + \psi_2$, and we directed $\boldsymbol{S}_+$ along $\hat{z}$. In terms of these variables, $R^2 = 3r^2(1+3\varepsilon^4/16[1-(1/9)\cos 4\theta] + O(\varepsilon^6))$. The result $F^{(4)} = -(7/3)|\beta|R^4$ is also valid up to $O(\varepsilon^6)$. The seven independent variables in (6), together with the requirement that R^2 is fixed, yield six Goldstone modes. This can also be shown more rigorously by noticing that for $\beta < 0$, SU(4) symmetry is broken down to SU(3) $\otimes$ U(1) [42]. The broken symmetry is described by the coset SU(4)/[SU(3) $\otimes$ U(1)] with $15-8-1=6$ generators, corresponding to the six Goldstone modes [38].

Reconstructed fermionic dispersion.—Upon gap opening, the initial fourfold (spin and valley) degeneracy of the electronic dispersion in the six- and two-patch model is lifted. For the six-patch model, we verified that the states remain doubly degenerate for any configuration from the order parameter manifold [38]. The easiest way to see this is to consider the state with s^{+-} valley order: it splits chemical potentials in the two valleys but preserves spin degeneracy. Similarly, the bands remain twofold degenerate also for spin and density-wave orders. For the two-patch model, the situation is different: a fourfold degenerate Fermi level splits into a nondegenerate level, which shifts by $3r/4$, and a threefold degenerate one, which shifts by $-r/4$ (see Fig. 3). Such a splitting is consistent with the residual SU(3) $\otimes$ U(1) symmetry and holds for any configuration from the order parameter manifold.

The sign of r is determined by $F^{(3)} = \gamma r^3$, where $\gamma = (-1/2)d^2n/d\mu^2$. This γ can be directly extracted from the data on compressibility $d\mu/dn$. The data at zero external field show [43] that at small n, $d\mu/dn$ decreases with increasing n, hence $\gamma < 0$, but for $n > 0.7$, the slope of $d\mu/dn$ changes sign, and for larger n, $\gamma > 0$. For a positive γ, the equilibrium value of r is negative. In this situation, a singly degenerate level moves down in energy, while three degenerate levels move up, see Fig. 3. Such a splitting implies that the mixed spin and valley order increases the filling of a band for fermions with a given valley and band index at the expense of three other bands, which get depleted. This, along with the behavior near $n = 2$, in which the filling of two bands increases and that of the other two bands decreases, is consistent in general terms with the scenario [43] of a cascade of phase transitions with consequent filling of the bands of fermions with given valley and spin indices.

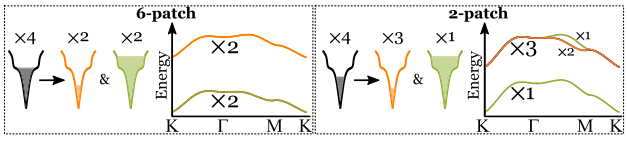

FIG. 3. Band splitting in the ground state (X labels degeneracy) An almost fourfold valley and spin degenerate band splits either into two twofold degenerate bands in the six-patch model, or into one threefold degenerate and one nondegenerate band in the two-patch model.

Conclusions.—In this work we described the formation of a symmetry-broken ground state in TBG near $n \approx 2$ and $n \approx 1$. We introduced two itinerant patch models: the two-patch model for $n \approx 1$, in which Fermi surfaces form pockets near Dirac points K, K', and the six-patch model for $n \approx 2$, which we associated with vH filling. We analyzed potential instabilities in the particle-hole channel and derived the corresponding Landau functionals. We argued that in both cases the largest and (almost) equal couplings are for a set of 15 order parameters. These 15 order parameters form an adjoint representation of SU(4), and the corresponding Landau functional is SU(4) symmetric. These order parameters represent spin and valley orders with zero and finite momentum transfer.

We found two different order parameter manifolds depending on whether the SU(4) symmetry is broken down to SU(2) $\otimes$ SU(2) $\otimes$ U(1), as in the six-patch model, or to SU(3) $\otimes$ U(1), as in the two-patch model. In the first case, the manifold has eight Goldstone modes, and the initially fourfold degenerate energy level splits into two doubly degenerate levels. In the second case the manifold has six Goldstones, and the fourfold degenerate level splits into one nondegenerate level and three degenerate ones. Because SU(4) is only approximate, some of the Goldstone modes are pseudo-Goldstones. Yet, this should preserve a qualitative difference between order-parameter manifolds near $n = 2$ and $n = 1$. We treated $n = 1$ and $n = 2$ instabilities separately. The next step in this analysis would be to consider the $n = 2$ instability, arising from the already ordered state, induced by the transition at $n = 1$. We also note that some of our results, like the splitting of energy levels ($4 \to 1+3$ and $4 \to 2+2$) and the number of Goldstone modes (eight and six), match the results for Chern insulators [21], although in our case the number of Goldstone modes is not directly related to the Chern numbers. Another similarity to strong-coupling approaches is the large number of degenerate ground states that we find due to the large symmetry. This has been discussed as a possible explanation for variations in experimental phase diagrams.

We thank R. Fernandes, L. Levitov, H. Polshyn, G. Tarnopolsky, O. Vafek, A. Vainshtein, and A. Vishwanath

for fruitful discussions. The work by D. V. C. and A. V. C. was supported by U.S. Department of Energy, Office of Science, Basic Energy Sciences, under Award No. DE-SC0014402. L. C. was supported by the U.S. Department of Energy (DOE), Office of Basic Energy Sciences, under Contract No. DE-SC0012704. Y. W. was supported by NSF under Award No. DMR-2045871. D. V. C. and A. V. C. also acknowledge the hospitality of KITP at Santa Barbara. The part of research done at KITP was supported in part by the National Science Foundation under Grant No. NSF PHY-1748958. D. V. C. gratefully acknowledges support from Doctoral Dissertation and Larkin Fellowships at the University of Minnesota.

[1] Y. Cao, V. Fatemi, A. Demir, S. Fang, S. L. Tomarken, J. Y. Luo, J. D. Sanchez-Yamagishi, K. Watanabe, T. Taniguchi, E. Kaxiras, R. C. Ashoori, and P. Jarillo-Herrero, Nature (London) **556**, 80 (2018).
[2] H. Polshyn, M. Yankowitz, S. Chen, Y. Zhang, K. Watanabe, T. Taniguchi, C. R. Dean, and A. F. Young, Nat. Phys. **15**, 1011 (2019).
[3] Y. Cao, V. Fatemi, S. Fang, K. Watanabe, T. Taniguchi, E. Kaxiras, and P. Jarillo-Herrero, Nature (London) **556**, 43 (2018).
[4] M. Yankowitz, S. Chen, H. Polshyn, Y. Zhang, K. Watanabe, T. Taniguchi, D. Graf, A. F. Young, and C. R. Dean, Science **363**, 1059 (2019).
[5] H. S. Arora, R. Polski, Y. Zhang, A. Thomson, Y. Choi, H. Kim, Z. Lin, I. Z. Wilson, X. Xu, J.-H. Chu, K. Watanabe, T. Taniguchi, J. Alicea, and S. Nadj-Perge, Nature (London) **583**, 379 (2020).
[6] Y. Saito, J. Ge, K. Watanabe, T. Taniguchi, and A. F. Young, Nat. Phys. **16**, 926 (2020).
[7] X. Lu, P. Stepanov, W. Yang, M. Xie, M. A. Aamir, I. Das, C. Urgell, K. Watanabe, T. Taniguchi, G. Zhang, A. Bachtold, A. H. MacDonald, and D. K. Efetov, Nature (London) **574**, 653 (2019).
[8] P. Stepanov, I. Das, X. Lu, A. Fahimniya, K. Watanabe, T. Taniguchi, F. H. L. Koppens, J. Lischner, L. Levitov, and D. K. Efetov, Nature (London) **583**, 375 (2020).
[9] A. L. Sharpe, E. J. Fox, A. W. Barnard, J. Finney, K. Watanabe, T. Taniguchi, M. A. Kastner, and D. Goldhaber-Gordon, Science **365**, 605 (2019).
[10] M. Serlin, C. L. Tschirhart, H. Polshyn, Y. Zhang, J. Zhu, K. Watanabe, T. Taniguchi, L. Balents, and A. F. Young, Science **367**, 900 (2020).
[11] Y. Saito, J. Ge, L. Rademaker, K. Watanabe, T. Taniguchi, D. A. Abanin, and A. F. Young, Nat. Phys. **17**, 478 (2021).
[12] D. Wong, K. P. Nuckolls, M. Oh, B. Lian, Y. Xie, S. Jeon, K. Watanabe, T. Taniguchi, B. A. Bernevig, and A. Yazdani, Nature (London) **582**, 198 (2020).
[13] K. P. Nuckolls, M. Oh, D. Wong, B. Lian, K. Watanabe, T. Taniguchi, B. A. Bernevig, and A. Yazdani, Nature (London) **588**, 610 (2020).
[14] I. Das, X. Lu, J. Herzog-Arbeitman, Z.-D. Song, K. Watanabe, T. Taniguchi, B. A. Bernevig, and D. K. Efetov, Nat. Phys. **17**, 710 (2021).
[15] S. Wu, Z. Zhang, K. Watanabe, T. Taniguchi, and E. Y. Andrei, Nat. Mater. **20**, 488 (2021).
[16] Y. Choi, H. Kim, Y. Peng, A. Thomson, C. Lewandowski, R. Polski, Y. Zhang, H. S. Arora, K. Watanabe, T. Taniguchi, J. Alicea, and S. Nadj-Perge, Nature (London) **589**, 536 (2021).
[17] Y. Saito, F. Yang, J. Ge, X. Liu, T. Taniguchi, K. Watanabe, J. I. A. Li, E. Berg, and A. F. Young, Nature (London) **592**, 220 (2021).
[18] J. Kang and O. Vafek, Phys. Rev. Lett. **122**, 246401 (2019).
[19] Y.-H. Zhang, D. Mao, Y. Cao, P. Jarillo-Herrero, and T. Senthil, Phys. Rev. B **99**, 075127 (2019).
[20] F. Xie, A. Cowsik, Z.-D. Song, B. Lian, B. A. Bernevig, and N. Regnault, Phys. Rev. B **103**, 205416 (2021).
[21] E. Khalaf, N. Bultinck, A. Vishwanath, and M. P. Zaletel, Soft modes in magic angle twisted bilayer graphene, arXiv:2009.14827.
[22] C. Repellin and T. Senthil, Phys. Rev. Research **2**, 023238 (2020).
[23] S. Liu, E. Khalaf, J. Y. Lee, and A. Vishwanath, Phys. Rev. Research **3**, 013033 (2021).
[24] J. Kang, B. A. Bernevig, and O. Vafek, Phys. Rev. Lett. **127**, 266402 (2021).
[25] P. Potasz, M. Xie, and A. H. MacDonald, Phys. Rev. Lett. **127**, 147203 (2021).
[26] Y. Choi, J. Kemmer, Y. Peng, A. Thomson, H. Arora, R. Polski, Y. Zhang, H. Ren, J. Alicea, G. Refael *et al.*, Nat. Phys. **15**, 1174 (2019).
[27] A. MacDonald, in *Talk at the KITP Rapid Response Workshop* (2019), https://online.kitp.ucsb.edu/online/bands_m19/macdonald/.
[28] Y.-P. Lin and R. M. Nandkishore, Phys. Rev. B **100**, 085136 (2019).
[29] D. V. Chichinadze, L. Classen, and A. V. Chubukov, Phys. Rev. B **101**, 224513 (2020).
[30] D. V. Chichinadze, L. Classen, and A. V. Chubukov, Phys. Rev. B **102**, 125120 (2020).
[31] Y. Wang, J. Kang, and R. M. Fernandes, Phys. Rev. B **103**, 024506 (2021).
[32] J. Kang and O. Vafek, Phys. Rev. X **8**, 031088 (2018).
[33] N. F. Q. Yuan and L. Fu, Phys. Rev. B **98**, 045103 (2018).
[34] M. Koshino, N. F. Q. Yuan, T. Koretsune, M. Ochi, K. Kuroki, and L. Fu, Phys. Rev. X **8**, 031087 (2018).
[35] B. A. Bernevig, Z.-D. Song, N. Regnault, and B. Lian, Phys. Rev. B **103**, 205413 (2021).
[36] N. F. Q. Yuan, H. Isobe, and L. Fu, Nat. Commun. **10**, 5769 (2019).
[37] For this to hold, it is important that the corresponding generators satisfy the orthonormal condition, which in our case is $\mathrm{Tr}[\sigma_i \otimes \tau_j, \sigma_{i'} \otimes \tau_{j'}] = 4\delta_{ii'}\delta_{jj'}$.
[38] See Supplemental Material at http://link.aps.org/supplemental/10.1103/PhysRevLett.128.227601 for details of calculations, which includes Ref. [39].
[39] R. Nandkishore, G.-W. Chern, and A. V. Chubukov, Phys. Rev. Lett. **108**, 227204 (2012).
[40] Two comments are in order. First, for a generic six-patch model, there are three types of fourth order terms, with three coefficients $\beta_1 = T\sum_{\omega_m} G_k^4$, $\beta_2 = T\sum_{\omega_m} G_k^3 G_{k+Q}$, and $\beta_3 = T\sum_{\omega_m} G_k^2 G_{k+Q}^2$, where $G_k = 1/(i\omega_m - \epsilon_k)$. All $\beta_i = \bar{\beta}_i/T^2$. For the parameters of the dispersion that we

use, all three $\bar{\beta}_i$ are close (see [38]), and we neglect the differences between them. In a two-patch model at $n \approx 1$, β_i is also not identical, but differs by even smaller amount. Second, SU(4) symmetry also permits a quartic term $\propto \mathrm{Tr}[\Phi^2]^2$, which is absent in the microscopic derivation of F. It would yield independent prefactors β, β' in $F^{(4)} = \beta' R^4 + 4\beta C$ in Eq. (3).

[41] Ferromagnetism and s^{+-} valley order break time-reversal symmetry, but antiferromagnetism preserves it. Because Cooper pairs are formed by fermions from different valleys (see Fig. 1), an antiferromagnetic alignment is not detrimental to spin-singlet superconductivity, while the other two orders are.

[42] N. Chen, T. A. Ryttov, and R. Shrock, Phys. Rev. D **82**, 116006 (2010).

[43] U. Zondiner, A. Rozen, D. Rodan-Legrain, Y. Cao, R. Queiroz, T. Taniguchi, K. Watanabe, Y. Oreg, F. von Oppen, A. Stern *et al.*, Nature (London) **582**, 203 (2020).